Letter

Understanding the Quality Factor of Mass-Loaded Tensioned Resonators

R. Shaniv,* S. Kumar Keshava, C. Reetz, and C.A. Regal
JILA, National Institute of Standards and Technology and University of Colorado, and Department of Physics, University of Colorado, Boulder, Colorado 80309, USA

(Received 11 September 2022; revised 9 February 2023; accepted 14 February 2023; published 29 March 2023)

Mechanical resonators featuring large tensile stress have enabled a range of experiments in quantum optomechanics and precision sensing. Many sensing applications require functionalizing tensioned resonators by appending additional mass to them. However, this may dramatically change the resonator mode quality factor, and hence its sensitivity. In this work, we investigate the effect of the crossover from no mass load to a large mass load on the mode shape and quality factor of a tensioned resonator. We show through an analytical model and finite element analysis that as the load mass increases, surprisingly, the resonator mode shape becomes independent of the exact load mass, and, therefore, the resonator mode quality factor saturates. We validate this saturation effect experimentally by measuring the quality factor of a tensioned silicon nitride trampoline resonator while varying the load mass in a controlled manner.

DOI: 10.1103/PhysRevApplied.19.L031006

Micromechanical and nanomechanical resonators have been a fruitful topic of research for several decades. They have shown promise for exploring quantum physics [1], in studies ranging from quantum transduction protocols [2–4] and creation of quantum memories [5–7] to the generation of squeezed light [8–10], and for precision sensing applications, such as microscopy [11] and mass sensing [12–14].

To couple a resonator sensor to a quantity of interest, it is often necessary to functionalize it with a coupling agent, resulting in an additional resonator mass. In some applications, the desired observable scales with the added mass, explicitly $D = \beta M$, where D, β, and M are the observable, quantity of interest, and mass, respectively. Examples include magnetic force sensing [15,16], accelerometry [17,18], and detection of gravitational forces [19–21]. Generally, specific interest is devoted to modes where the mass moves appreciably. For a large mass, typically, there is only one such mode, and it is usually the lowest-frequency or fundamental mode. The fundamental sensitivity for the evaluation of β in this mode is [17]

$$S_\beta = \sqrt{\frac{4k_B T\omega}{MQ}}, \tag{1}$$

where k_B, T, ω, M, and Q are the Boltzmann constant, temperature, mechanical mode resonance frequency, added mass, and mode quality factor, respectively. For best sensitivity, it is therefore desired to maximize the figure of merit $s = MQ/\omega$, and therefore it is imperative to understand the dependence of Q on M.

The Q of a resonator mode is defined as $Q = 2\pi W/\Delta W$, where W is the energy stored in the mode and ΔW is the energy loss per oscillatory cycle [22,23]. Generally, ΔW is a sum of contributions from multiple loss mechanisms [23,24]. One way to improve the Q of a resonator is to increase the stored energy without a similar increase in dissipation. This can be achieved by using a tensioned or high-stress film and results in the phenomenon known as dissipation dilution [25–27]. High stress also extends the resonator mode spectrum to higher frequencies for a given resonator length scale. High frequency is of interest for certain sensing protocols, while being out of reach for similar-length-scale nontensioned resonators such as cantilevers.

Low optical absorption combined with high stress obtained in fabrication make silicon nitride (SiN) a natural material for high-Q resonator design [28–31]. In tensioned SiN resonator modes, typically, Q is limited by two loss mechanisms—bending loss, which is the energy lost due to mode bending, and radiation loss, which is the energy lost from the mode into the surroundings via acoustic radiation. We define individual quality factors, Q_{bend} and Q_{rad}, associated with bending loss and radiation loss, respectively, such that $1/Q = 1/Q_{\text{bend}} + 1/Q_{\text{rad}}$. We omit loss from resonator elongation, which is reasonable for small resonator amplitudes [32]. Q_{bend} can be significantly improved by tailoring the mode shape to reduce bending loss at the mode edge, commonly referred to as clamping loss [26,27,33–38]. Q_{rad} can be improved by resonator patterning, substrate engineering, and strategic device mounting [26,33,38–45]. These techniques have led to resonators with modes limited by Q_{bend}.

In this work, we study the effect of a localized mass load on Q_{bend} of highly tensioned resonators. We show

*ravid.shaniv@gmail.com

through analytical calculations and finite-element analysis (FEA) that as the load mass increases, the modes of the resonator change in frequency and shape. Further, we show that for a large enough mass, each mode shape becomes independent of the mass, which leads to mass-independent Q_{bend}. We refer to this phenomenon as Q_{bend} *mass saturation*. A direct result of Q_{bend} mass saturation is the scaling $s \propto M^{3/2}$, suggesting that at the large-mass limit, the sensitivity scales favorably with mass. This could also explain other experimental results, for example in Ref. [19], where a surprisingly high Q (6.4×10^5) was measured for a highly massive (approximately 1.3 mg) tensioned resonator mode. We validate this saturation experimentally by measuring the Q of a tensioned SiN trampoline resonator [35,37] as a function of the load mass. We use magnetic grains for the load mass, and we vary the mass by sequentially stacking the grains using their mutual magnetic attraction to avoid varying the amount of lossy adhesive used. This allows us to compare Q measurements for different load masses on a single device.

To obtain an expression for the Q_{bend} of a mode, we assume pure out-of-plane mode displacement $u(x,y)$, where x and y are in-plane resonator coordinates, as well as small displacement $|u(x,y)| \ll h$, where h is the resonator thickness. In addition, we assume large in-plane tensile stress σ_0, such that the speed of sound along the resonator is approximately proportional to $\sqrt{\sigma_0}$. Then we can write

$$W \approx \int_V \frac{\sigma_0}{2}\left[\left(\frac{\partial u}{\partial x}\right)^2 + \left(\frac{\partial u}{\partial y}\right)^2\right] dV$$

and

$$\Delta W_{\text{bend}} \approx \int_V \frac{\pi E_2}{(1-\nu^2)} z^2 \left[\frac{\partial^2 u}{\partial x^2} + \frac{\partial^2 u}{\partial y^2}\right]^2 dV,$$

where E_2 is the imaginary part of the Young modulus, ν is the Poisson ratio, z is the resonator coordinate along its thickness, and V is the volume of the resonator [26,46]. This leads to

$$Q_{\text{bend}}(u) = \frac{\int_V \sigma_0 \left[\left(\frac{\partial u}{\partial x}\right)^2 + \left(\frac{\partial u}{\partial y}\right)^2\right] dV}{\int_V \frac{E_2}{(1-\nu^2)} z^2 \left[\frac{\partial^2 u}{\partial x^2} + \frac{\partial^2 u}{\partial y^2}\right]^2 dV}. \tag{2}$$

Equation (2) affirms that if $u(x,y)$ is independent of the load mass, then Q_{bend} saturates.

Although it applies to general tensioned resonator geometry, we elucidate this Q_{bend} saturation and its origin through a *minimal* model example, chosen to be in 1D for brevity. We study the fundamental mode of a highly tensioned suspended beam, referred to as a string, with a mass load. The string resonator is fixed at both ends, with displacement $u(x)$ in the vertical axis, where x is the coordinate along the resonator [Fig. 1(a)]. Here $u(x)$ satisfies the string equation [24]:

$$\frac{Eh^2}{12\sigma_0}\frac{d^4u}{dx^4} - \frac{d^2u}{dx^2} - \frac{\rho(x)(2\pi f)^2}{\sigma_0}u = 0, \tag{3}$$

for $0 \le x \le L$, where L is the string length. Here, E, h, and σ_0 are the string's Young's modulus, thickness, and tensile stress, respectively, and f is the mode frequency. The string width w is absent from Eq. (3) because the string has a uniform width. The position-dependent density $\rho(x)$ accounts for possible increased density at some

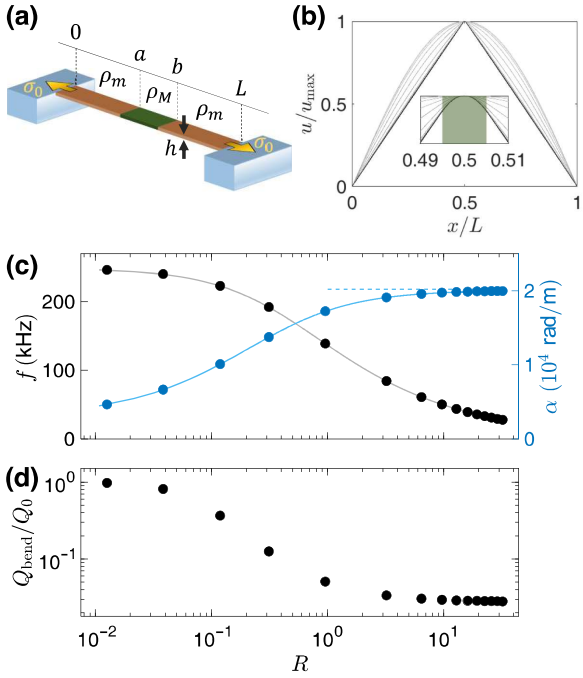

FIG. 1. Mass-loaded-string theoretical model. (a) String parameters: a string of length L and thickness h with tensile stress σ_0 is fixed at the edges $x = 0$ and $x = L$, and has linear density ρ_m everywhere except for the region $a \le x \le b$, where the density is $\rho_M + \rho_m$. (b) Mode shape visualization: FEA simulations of the mass-loaded-string fundamental mode normalized to its maximum displacement (lighter color corresponds to lighter mass load). Inset: mode shape at the loaded region (shaded green). (c) String frequency and inner region wave number: FEA simulated (solid circles) and analytically calculated (solid lines) fundamental mode frequency (black) and inner region wave number (blue) are shown as a function of R, the ratio between load mass and total mass of the unloaded resonator, scanned by varying ρ_M while keeping a and b constant. Simulation points correspond to the mode shapes in (b). Dashed blue line is the analytically calculated large-mass limit inner region wave number α_{lim}. (d) String quality factor: fundamental mode Q_{bend} normalized to Q_0, the Q_{bend} of an unloaded resonator, as a function of R. To focus on mass loading effects, Q_{bend} is calculated neglecting edge clamping loss. Panels (c),(d) share the horizontal coordinate, and results shown correspond to specific choice of parameters [47].

region $a \le x \le b$, for $0 < a < b < L$. We denote the density at $0 \le x < a$ and $b < x \le L$, subsequently referred to as the outer regions, by ρ_m, and the density at $a \le x \le b$, the inner region, by $\rho_m + \rho_M$, such that ρ_M is the added density. The prestress σ_0 is assumed to be large, satisfying the length-scale inequality $l = 2\pi\sqrt{Eh^2/12\sigma_0} \ll L$. We now show that large inner region density suffices for Q saturation.

Given this high prestress, the frequency of the string's fundamental mode can be well approximated by neglecting the fourth derivative term in Eq. (3) [24]. The solution then reads

$$u(x) = \begin{cases} A_1 \sin\left(\frac{\alpha}{\sqrt{1+\chi}}x\right) & 0 \le x \le a, \\ A_2 \sin(\alpha x) + B_2 \cos(\alpha x) & a \le x \le b, \\ A_3 \sin\left(\frac{\alpha}{\sqrt{1+\chi}}(L-x)\right) & b \le x \le L, \end{cases} \quad (4)$$

where we introduce the density ratio $\chi = \rho_M/\rho_m$ and the inner region wave number $\alpha = 2\pi f\sqrt{(\rho_m + \rho_M)/\sigma_0}$, and impose the fixed boundary conditions $u(0) = u(L) = 0$. An equation for α can be found by using the continuity of $u(x)$ and its first derivative at $x = a$ and $x = b$ [47]. We see excellent agreement [Fig. 1(c)] between FEA simulations of α and f, and the corresponding numerically evaluated analytical calculation, for different values of R, the resonator mass ratio, defined as $R = M_{\text{load}}/M_{\text{unloaded}}$. Here, $M_{\text{load}} = hw(b-a)(\rho_M)$ and $M_{\text{unloaded}} = hwL\rho_m$ correspond to the load mass and the total unloaded resonator mass, respectively. This parameter is scanned by varying ρ_M, and is chosen to emphasize that we are investigating the crossover between no load ($R = 0$) and a load significantly larger than the entire resonator mass ($R \gg 1$).

In addition to α and f, we use the FEA simulation results for the fundamental mode along with Eq. (2) to calculate Q_{bend}/Q_0 as a function of R [Fig. 1(d)]. Here, Q_0 is Q_{bend} in the unloaded resonator. To focus on the effect of the load mass, we exclude the mechanical clamping loss contribution from the resonator edges. We find that Q_{bend}/Q_0 becomes independent of the exact load mass for $R \gg 1$ and it saturates to a value lower than when $R \approx 0$.

Figure 1(b) evinces that the fundamental mode inner region wave number α saturates to a finite value, α_{lim}, as the mass grows larger [47]. Simultaneously, the outer region wave number diminishes, and in the large-mass limit the mass-loaded-string equation can be approximated as

$$\frac{l^2}{(2\pi)^2}\frac{d^4u}{dx^4} - \frac{d^2u}{dx^2} - K^2(x)u = 0, \quad (5)$$

where

$$K^2(x) \approx \begin{cases} 0 & 0 \le x < a, \quad b < x \le L, \\ \alpha_{\text{lim}}^2 & a \le x \le b. \end{cases} \quad (6)$$

Because Eq. (5) is independent of the load mass, so is its solution [47].

This analysis assumes only larger density at the loaded region, while real mass loading should account for, for example, different elasticity constants or different internal modes. The internal loss in the mass should be added to the resonator bending loss. However, the prediction of Q_{bend} saturation holds as long as the resonator mode *including the mass* saturates. This is true when the internal mode structure of the load has higher resonances than the loaded resonator mode. In that case, the load approximates a rigid body moving uniformly with the resonator.

In the large-mass limit, the shape of the unloaded regions can be understood in two equivalent ways. The first is temporal: for an unloaded resonator, the fundamental mode period is given by $T_{\text{unloaded}} = \sqrt{(\rho_m)/(\sigma_0)}2L$, which is the time it takes an out-of-plane mechanical perturbation to make a roundtrip across a resonator of length L, with speed of sound $\sqrt{\sigma_0/\rho_m}$. As the high-mass load limit is approached ($\rho_m \to \rho_m + \rho_M$), the mode period increases to T_{loaded}, which is now much longer than the roundtrip time taken for a perturbation to propagate in the unloaded regions. As a result, the mode shape in the unloaded region approximates a quasistatic displacement, with the limit shape being a static displacement at any moment. The second explanation is spatial: in the limit of a large load mass, the mode wavelength in the unloaded region, $T_{\text{loaded}}\sqrt{\sigma_0/\rho_m}$, is much longer than the unloaded region length scale. As a result, the mode shape converges to a displacement function that does not curve in the unloaded region. For a string, the resulting limit shape is linear in the outer regions, and since the inner region has to match with the outer regions at the boundaries, the overall mode approaches a limit shape that is approximately triangular [Fig. 1(b)]. This leads to the splitting of the string equation in Eqs. (5) and (6), and as explained, its solution is independent of the load mass, implying Q_{bend} saturation.

Although our analysis thus far focuses on the case of the mass-loaded string, the key points of the explanation above apply to highly tensioned resonators of arbitrary geometry and imply Q_{bend} saturation for a high enough mass load. Specifically, as an example we also analyze a loaded circular membrane [47].

To validate the model-predicted Q_{bend} saturation experimentally, we measure the fundamental mode Q, denoted hereafter as Q_{fund}, of a high-stress SiN trampoline resonator [35,37] for different load masses. A trampoline resonator features a wide pad for low-imprecision optical detection and the geometry is designed to reduce mechanical clamping and radiation losses [35,37]. Our device is

mounted on a custom-made silicon base to minimize radiation loss. This setup ensures $Q_{\text{rad}} \gg Q_{\text{bend}}$ for an unloaded trampoline fundamental mode, and thus allows $Q_{\text{fund}} \approx Q_{\text{bend}}$ [47].

In order to vary the load mass while keeping other variables constant, we employ a "magnetic stacking" technique using magnetic particles as the load mass. The first particle is affixed to our device using ultraviolet-cured epoxy (NEA 123SHGA) [Fig. 2(a)] and then magnetized using an external field. Next, a second particle is brought near the first, resulting in magnetic attraction between the particles. A magnetizing field is applied once again to magnetize the second particle, making both particles a single, inseparable mass without using additional epoxy. This procedure is repeated [Fig. 2(c)] and Q_{fund} is measured between each addition of mass. Although we expect the epoxy to have high mechanical loss compared with SiN, by keeping its geometry constant through magnetic stacking, we can study how Q_{fund} changes with mass loading while avoiding errors associated with multiple epoxy applications. We find that loading the tether yields higher Q_{bend} compared with the trampoline pad [47].

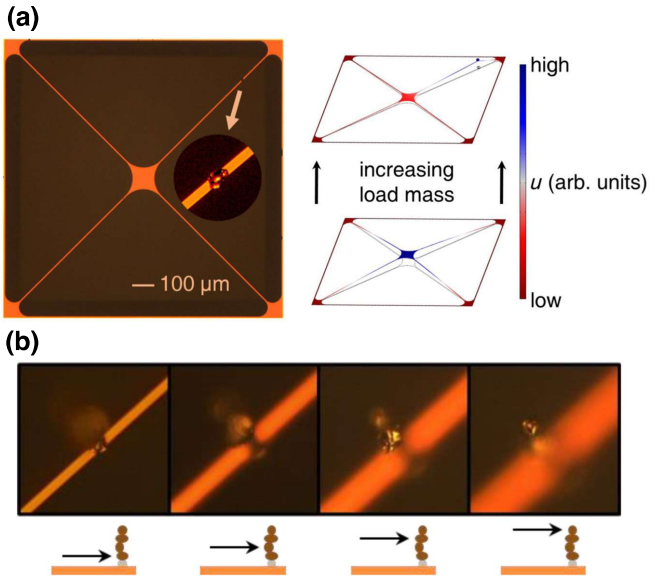

FIG. 2. System for experimental validation. (a) Microscope image of device: trampoline resonator with a magnet on its tether. Inset: enlarged magnet image. (b) Mode visualization: FEA simulations of trampoline loaded (top) and unloaded (bottom) fundamental mode shape. Simulations show that the unloaded mode continuously deforms into the high-load-limit mode as load mass increases. (c) Magnetic stacking: images in different planes of focus show a stack of four magnets, from the first magnet in focus (leftmost image) to the fourth magnet in focus (rightmost image). The schematic at the bottom shows a side view of the trampoline resonator (orange slab), droplet of epoxy (gray dot), and magnets (dark brown dot). Each drawing indicates the magnet in focus in the corresponding image (black arrow pointing at dark brown dot).

The key experimental results are shown in Fig. 3(a) along with relevant FEA simulations. Open black circle and filled black circles correspond to the measured Q_{fund} values for a trampoline resonator at 300 K, without and with a variable load mass, respectively. As visible, Q_{fund} decreases as the load mass increases, but becomes insensitive at higher load mass values. This is manifested as a plateau for masses larger than approximately 10 ng. This saturated Q_{fund} value is approximately 4 orders of magnitude lower than the unloaded Q_{fund} value. To model these results, we use FEA simulations that account for bending loss in both the SiN and the epoxy, while disregarding radiation loss (black dotted line). We scan the epoxy length scale and loss tangent and choose realistic model parameters to obtain reasonable agreement between our simulation results and measured data, while also setting an upper bound on Q_{fund} [47]. Our simulation is used as an upper bound for the results as, irrespective of device mounting, at higher mass (lower frequency), the resonator is more susceptible to radiation loss.

In order to further validate that the large reduction in Q_{fund} originates mainly from loss in the epoxy rather than radiation loss, we perform additional measurements on two different devices (triangle and square) both at temperatures of 300 and 8 K (light pink and sky blue markers, respectively). The measured Q_{fund} rises by 2 orders of magnitude

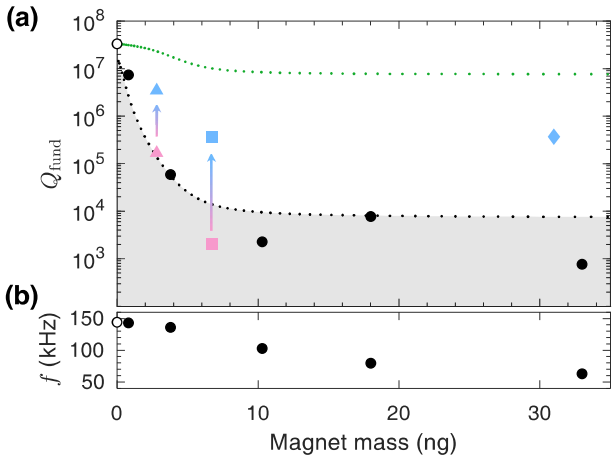

FIG. 3. Experimental results and FEA simulations. (a) Q_{fund} as a function of magnet mass: measured Q_{fund} at 300 K (circles) unloaded (open circle) and with a varying load (filled circles). Corresponding FEA simulated Q_{bend} results disregarding (green dotted line) and including (black dotted line) epoxy loss. The shaded area accounts for other possible losses, e.g. radiation loss. Measured Q_{fund} for two additional devices (triangle and square) are shown at both 300 K (light pink) and 8 K (sky blue). Measured Q_{fund} for a third device with a large load mass at 8 K is also shown (sky blue diamond). (b) Fundamental mode frequency as a function of magnet mass: frequency measurements at 300 K (circles) corresponding to data points in (a).

for resonators cooled to 8 K. Although SiN resonators are expected to have reduced bending loss at 8 K compared with 300 K, empirically it is by a small factor of approximately 3, which cannot explain these observations [33]. We therefore conclude that when cold, the epoxy loss reduces significantly, affirming that the reduction in Q_{fund} is primarily due to loss in the epoxy.

A fourth device (sky blue diamond) measured at 8 K provides evidence that a fairly high quality factor ($Q_{\text{fund}} \approx 3.7 \times 10^5$) can be achieved in the saturated regime. This is in agreement with measurements from Ref. [19].

In order to set a theoretical limit on the saturated Q_{fund} at 300 K, we perform FEA simulations that include only SiN bending loss and disregard all other forms of loss (green dotted line). The results indicate that Q_{bend} as high as 10^7 is possible in the limit of a large load mass. The saturated Q_{bend} for trampolines can be improved with mass load location optimization [47] and possibly by using trampoline resonators with carefully engineered geometries [35,37,48].

In conclusion, we analyze the problem of tensioned mechanical resonators with a local mass load. We demonstrate theoretically and experimentally that for a large load mass, the mode shape becomes independent of the mass and converges to a limit shape, implying Q_{bend} saturation and favorable sensitivity scaling for mass-dependent signals. As a rule of thumb, for localized load we observe that this happens when the load mass is of the order of the unloaded resonator mass. We believe that this work provides important guiding principles for sensor design where mass loading is needed.

Acknowledgments.—We thank Maxwell Urmey for helpful comments on the manuscript and David Carlson for fabrication expertise. This work is supported by funding from NSF Grant No. PHYS 1734006, Cottrell FRED Award from the Research Corporation for Science Advancement under Grant No. 27321, the CU UROP program, and the Baur-SPIE Endowed Professor at JILA. R.S. acknowledges support from the Israel Council for Higher Education.

[1] M. Aspelmeyer, T. Kippenberg, and F. Marquardt, Cavity optomechanics, Rev. Mod. Phys. **86**, 1391 (2014).

[2] R. Andrews, R. Peterson, T. Purdy, K. Cicak, R. Simmonds, C. Regal, and K. Lehnert, Bidirectional and efficient conversion between microwave and optical light, Nat. Phys. **10**, 321 (2014).

[3] M. Forsch, R. Stockill, A. Wallucks, I. Marinković, C. Gärtner, R. Norte, F. Otten, A. Fiore, K. Srinivasan, and S. Gröblacher, Microwave-to-optics conversion using a mechanical oscillator in its quantum ground state, Nat. Phys. **16**, 69 (2020).

[4] M. Mirhosseini, A. Sipahigil, M. Kalaee, and O. Painter, Superconducting qubit to optical photon transduction, Nature **588**, 599 (2020).

[5] A. Wallucks, I. Marinković, B. Hensen, R. Stockill, and S. Gröblacher, A quantum memory at telecom wavelengths, Nat. Phys. **16**, 772 (2020).

[6] P. Kharel, Y. Chu, M. Power, W. Renninger, R. Schoelkopf, and P. Rakich, Ultra-high-Q phononic resonators on-chip at cryogenic temperatures, Apl Photonics **3**, 066101 (2018).

[7] G. MacCabe, H. Ren, J. Luo, J. Cohen, H. Zhou, A. Sipahigil, M. Mirhosseini, and O. Painter, Nano-acoustic resonator with ultralong phonon lifetime, Science **370**, 840 (2020).

[8] T. Purdy, P. Yu, R. Peterson, N. Kampel, and C. Regal, Strong optomechanical squeezing of light, Phys. Rev. X **3**, 031012 (2013).

[9] A. Safavi-Naeini, S. Gröblacher, J. Hill, J. Chan, M. Aspelmeyer, and O. Painter, Squeezed light from a silicon micromechanical resonator, Nature **500**, 185 (2013).

[10] D. Brooks, T. Botter, S. Schreppler, T. Purdy, N. Brahms, and D. Stamper-Kurn, Non-classical light generated by quantum-noise-driven cavity optomechanics, Nature **488**, 476 (2012).

[11] P. Eaton and P. West, *Atomic Force Microscopy* (Oxford University Press, New York, 2010).

[12] Y. Yang, C. Callegari, X. Feng, K. Ekinci, and M. Roukes, Zeptogram-scale nanomechanical mass sensing, Nano Lett. **6**, 583 (2006).

[13] K. Ekinci, X. Huang, and M. Roukes, Ultrasensitive nanoelectromechanical mass detection, Appl. Phys. Lett. **84**, 4469 (2004).

[14] N. Lavrik and P. Datskos, Femtogram mass detection using photothermally actuated nanomechanical resonators, Appl. Phys. Lett. **82**, 2697 (2003).

[15] D. Rugar, R. Budakian, H. Mamin, and B. Chui, Single spin detection by magnetic resonance force microscopy, Nature **430**, 329 (2004).

[16] R. Fischer, D. McNally, C. Reetz, G. Assumpcao, T. Knief, Y. Lin, and C. Regal, Spin detection with a micromechanical trampoline: Towards magnetic resonance microscopy harnessing cavity optomechanics, New J. Phys. **21**, 043049 (2019).

[17] A. Krause, M. Winger, T. Blasius, Q. Lin, and O. Painter, A high-resolution microchip optomechanical accelerometer, Nat. Photonics **6**, 768 (2012).

[18] F. Zhou, Y. Bao, R. Madugani, D. Long, J. Gorman, and T. LeBrun, Broadband thermomechanically limited sensing with an optomechanical accelerometer, Optica **8**, 350 (2021).

[19] Y. Liu, J. Mummery, J. Zhou, and M. Sillanpää, Gravitational Forces Between Nonclassical Mechanical Oscillators, Phys. Rev. Appl. **15**, 034004 (2021).

[20] J. Schmöle, M. Dragosits, H. Hepach, and M. Aspelmeyer, A micromechanical proof-of-principle experiment for measuring the gravitational force of milligram masses, Classical Quantum Gravity **33**, 125031 (2016).

[21] J. Pratt, A. Agrawal, C. Condos, C. Pluchar, S. Schlamminger, and D. Wilson, Nanoscale torsional dissipation dilution for quantum experiments and precision measurement. ArXiv Preprint ArXiv:2112.08350 (2021).

[22] J. Taylor, Classical Mechanics. 3 "E ed. (Print).
[23] L. LD and E. LIFSHITZ, *Course of Theoretical Physics. Theory Of Elasticity,* (Pergamon, Oxford, UK, 1975).
[24] S. Schmid, L. Villanueva, and M. Roukes, *Fundamentals of Nanomechanical Resonators* (Springer International Publishing, Vienna, Austria, 2016).
[25] S. Fedorov, N. Engelsen, A. Ghadimi, M. Bereyhi, R. Schilling, D. Wilson, and T. Kippenberg, Generalized dissipation dilution in strained mechanical resonators, Phys. Rev. B **99**, 054107 (2019).
[26] Y. Tsaturyan, A. Barg, E. Polzik, and A. Schliesser, Ultracoherent nanomechanical resonators via soft clamping and dissipation dilution, Nat. Nanotechnol. **12**, 776 (2017).
[27] A. Ghadimi, S. Fedorov, N. Engelsen, M. Bereyhi, R. Schilling, D. Wilson, and T. Kippenberg, Elastic strain engineering for ultralow mechanical dissipation, Science **360**, 764 (2018).
[28] B. Zwickl, W. Shanks, A. Jayich, C. Yang, A. Bleszynski Jayich, J. Thompson, and J. Harris, High quality mechanical and optical properties of commercial silicon nitride membranes, Appl. Phys. Lett. **92**, 103125 (2008).
[29] M. Yuan, M. Cohen, and G. Steele, Silicon nitride membrane resonators at millikelvin temperatures with quality factors exceeding 108, Appl. Phys. Lett. **107**, 263501 (2015).
[30] E. Serra, M. Bawaj, A. Borrielli, G. Di Giuseppe, S. Forte, N. Kralj, N. Malossi, L. Marconi, F. Marin, F. Marino, B. Morana, R. Natali, G. Pandraud, A. Pontin, G. A. Prodi, M. Rossi, P. M. Sarro, D. Vitali, and M. Bonaldi, Microfabrication of large-area circular high-stress silicon nitride membranes for optomechanical applications, AIP Adv. **6**, 065004 (2016).
[31] L. Villanueva and S. Schmid, Evidence of Surface Loss as Ubiquitous Limiting Damping Mechanism in SiN Micro- and Nanomechanical Resonators, Phys. Rev. Lett. **113**, 227201 (2014).
[32] Q. Unterreithmeier, T. Faust, and P. Jörg, Damping of Nanomechanical Resonators, Phys. Rev. Lett. **105**, 027205 (2010).
[33] C. Reetz, R. Fischer, G. Assumpcao, D. McNally, P. Burns, J. Sankey, and C. Regal, Analysis of Membrane Phononic Crystals with Wide Band Gaps and Low-Mass Defects, Phys. Rev. Appl. **12**, 044027 (2019).
[34] M. Bereyhi, A. Beccari, S. Fedorov, A. Ghadimi, R. Schilling, D. Wilson, N. Engelsen, and T. Kippenberg, Clamp-tapering increases the quality factor of stressed nanobeams, Nano Lett. **19**, 2329 (2019).
[35] C. Reinhardt, T. Müller, A. Bourassa, and J. Sankey, Ultralow-noise SiN trampoline resonators for sensing and optomechanics, Phys. Rev. X **6**, 021001 (2016).
[36] S. Fedorov, A. Beccari, N. Engelsen, and T. Kippenberg, Fractal-like Mechanical Resonators with a Soft-Clamped Fundamental Mode, Phys. Rev. Lett. **124**, 025502 (2020).
[37] R. Norte, J. Moura, and S. Gröblacher, Mechanical Resonators for Quantum Optomechanics Experiments at Room Temperature, Phys. Rev. Lett. **116**, 147202 (2016).
[38] A. Ghadimi, D. Wilson, and T. Kippenberg, Radiation and internal loss engineering of high-stress silicon nitride nanobeams, Nano Lett. **17**, 3501 (2017).
[39] P. Yu, K. Cicak, N. Kampel, Y. Tsaturyan, T. Purdy, R. Simmonds, and C. Regal, A phononic bandgap shield for high-Q membrane microresonators, Appl. Phys. Lett. **104**, 023510 (2014).
[40] M. Weaver, B. Pepper, F. Luna, F. Buters, H. Eerkens, G. Welker, B. Perock, K. Heeck, S. Man, and D. Bouwmeester, Nested trampoline resonators for optomechanics, Appl. Phys. Lett. **108**, 033501 (2016).
[41] R. Norte, Nanofabrication for On-Chip Optical Levitation, Atom-Trapping, and Superconducting Quantum Circuits. *PhD Thesis*. (2015).
[42] D. Wilson, Cavity Optomechanics with High-Stress Silicon Nitride Films. *PhD Thesis*. (2012).
[43] C. Reinhardt, Ultralow-Noise Silicon Nitride Trampoline Resonators for Sensing and Optomechanics. *PhD Thesis*. (2017).
[44] A. Borrielli, L. Marconi, F. Marin, F. Marino, B. Morana, G. Pandraud, A. Pontin, G. Prodi, P. Sarro, E. Serra, and M. Bonaldi, Control of recoil losses in nanomechanical SiN membrane resonators, Phys. Rev. B **94**, 121403 (2016).
[45] Z. Li, Q. Zhang, X. You, Y. Li, and K. Peng, Suppression of phonon tunneling losses by microfiber strings for high-Q membrane microresonators, Appl. Phys. Lett. **109**, 191903 (2016).
[46] P. Yu, T. Purdy, and C. Regal, Control of Material Damping in High-Q Membrane Microresonators, Phys. Rev. Lett. **108**, 083603 (2012).
[47] See Supplemental Material at http://link.aps.org/supplemental/10.1103/PhysRevApplied.19.L031006 for further details regarding the theoretical, computational, and experimental details of this work on mass-loaded tensioned resonators.
[48] D. Høj, F. Wang, W. Gao, U. Hoff, O. Sigmund, and U. Andersen, Ultra-coherent nanomechanical resonators based on inverse design, Nat. Commun. **12**, 1 (2021).